Pergamon

Journal of Structural Geology, Vol. 18, No. 11, pp. 1301 to 1314, 1996

0191-8141/96 $15.00 + 0.00

PII: S0191-8141(96)00048-X

Modelling palaeostress magnitude and age in extensional basins: a case study from the Mesozoic Bristol Channel Basin, U.K.

MICHAL NEMCOK and ROD GAYER

Laboratory for Strain Analysis, Department of Earth Sciences, University of Wales Cardiff, P.O. Box 914, Cardiff CF1 3YE, U.K.

(*Received* 31 *January* 1994; *accepted in revised form* 30 *May* 1996)

Abstract—Analysis of normal faults and extensional veins developed in the Upper Triassic and Lower Jurassic succession exposed along the Bristol Channel coast indicate a protracted period of rift-related deformation, from Late Triassic to Early Cretaceous. During this period it is demonstrated that a consistently oriented stress system operated with σ_3 oriented NE–SW, but with stress ratios ($\phi = (\sigma_2 - \sigma_3)/(\sigma_1 - \sigma_3)$) varying from 0.9–0.1.

Two approaches are described to estimate rifting stress magnitudes. The first involves data from synsedimentary faults, and yields, for Late Triassic rifting, $\sigma_1 = 0.714$ MPa, $\sigma_2 = 0.169$ MPa and $\sigma_3 = 0.033$ MPa. The second is developed for faulting in the Lower Jurassic section, where no direct evidence of age is available. The method calculates stress magnitudes, with the rifting stress ratio of 0.9, for varying increments of overburden load. Each increment represents the possible magnitude of tectonic stresses at the time indicated by the amount of burial. By incrementally adding the estimated remaining Lower Jurassic–Lower Cretaceous overburden load to the stress magnitudes of each case, a plot of reducing stress ratio for each age of faulting is determined, and that which best reproduces the range of stress ratios calculated represents the modelled estimate of stress magnitude and timing. The results suggest an end Early Jurassic onset of faulting, with principal stress magnitudes of $\sigma_1 = 12.98$ MPa, $\sigma_2 = 12.56$ MPa, $\sigma_3 = 8.80$ MPa. Several simplifying assumptions used in the analysis are discussed. Copyright © 1996 Elsevier Science Ltd

INTRODUCTION

Normal faults associated with extensional sedimentary basins may record a spectrum of movement histories, from those active throughout the entire period of basin development, to those with only one slip event. Provided the sedimentary fill had become sufficiently lithified and brittle, these events will be preserved as discrete slickenside surfaces containing lineations that record the slip-vector of the fault event. Unless clear evidence relating the fault activity to synsedimentary growth is present, it is not generally possible to date a faulting event to any particular stage of the extensional history of a basin. Such information, however, could be highly significant for two important reasons: firstly it would help in understanding the tectonic development of a basin; and secondly it would indicate periods when fluids, such as hydrocarbons, may have migrated along fractures which were opened during fault activity.

This paper describes a technique for analysing palaeostress developed in an extensional basin, such that both the magnitudes of the principal tectonic stresses, and the stage within the basin development when a particular set of faults were active can be determined. The technique has been developed for the Inner Bristol Channel Basin (Fig. 1), where Triassic to Early Cretaceous rifting was followed by Early to Late Cretaceous quiescence, and Early Tertiary inversion (Kamerling 1979, Nemcok *et al.* 1995).

The Bristol Channel basin is one of a connected series of rift-related Mesozoic basins that extend east–west across southern England to the Celtic Sea (Chadwick 1986, Lake & Karner 1987). These were initiated during the Permo–Triassic by NW–SE extension (Van Hoorn 1987, Chadwick & Smith 1988, Nemcok *et al.* 1995), and rifting continued throughout the Jurassic into the Early Cretaceous (Aptian) with NE–SW extension (Ziegler 1989, Nemcok *et al.* 1995). During this period the Bristol Channel basin received some 1–2 km of shallow-water, largely calcareous sediments, accommodated by active rifting in an E–W trending half-graben (Nemcok *et al.* 1995) (Fig. 1). In many cases the controlling normal faults reactivated basement Variscan structures (Brooks *et al.* 1988, Nemcok *et al.* 1995). There is evidence for synsedimentary growth on some of the faults during the Late Triassic (Norian) and Jurassic (Hettangian and Sinemurian), but a major period of erosion during the Late Cretaceous, prior to Early Tertiary basin inversion, and inversion-related erosion removed the onshore record of later Mesozoic synsedimentary extensional activity (Nemcok *et al.* 1995). The palaeostress analysis presented in this paper aims to demonstrate that active extensional faulting continued into this younger Mesozoic interval with essentially constant stress magnitudes.

GEOLOGICAL SETTING

The Mesozoic rocks that crop out along the north and south coasts of the Bristol Channel (Fig. 1) represent a succession comprising > 160 m of Upper Triassic (Norian and Rhaetian) sediments overlain by > 150 m of Lower Jurassic (Hettangian and Sinemurian) sediments (Waters *et al.* 1987). The Upper Triassic succession is formed dominantly of non-marine red and green calcareous mudstones with evaporites (the Mercia Mudstone Group) that pass laterally into a variable marginal facies of breccias, conglomerates and sandstones. The

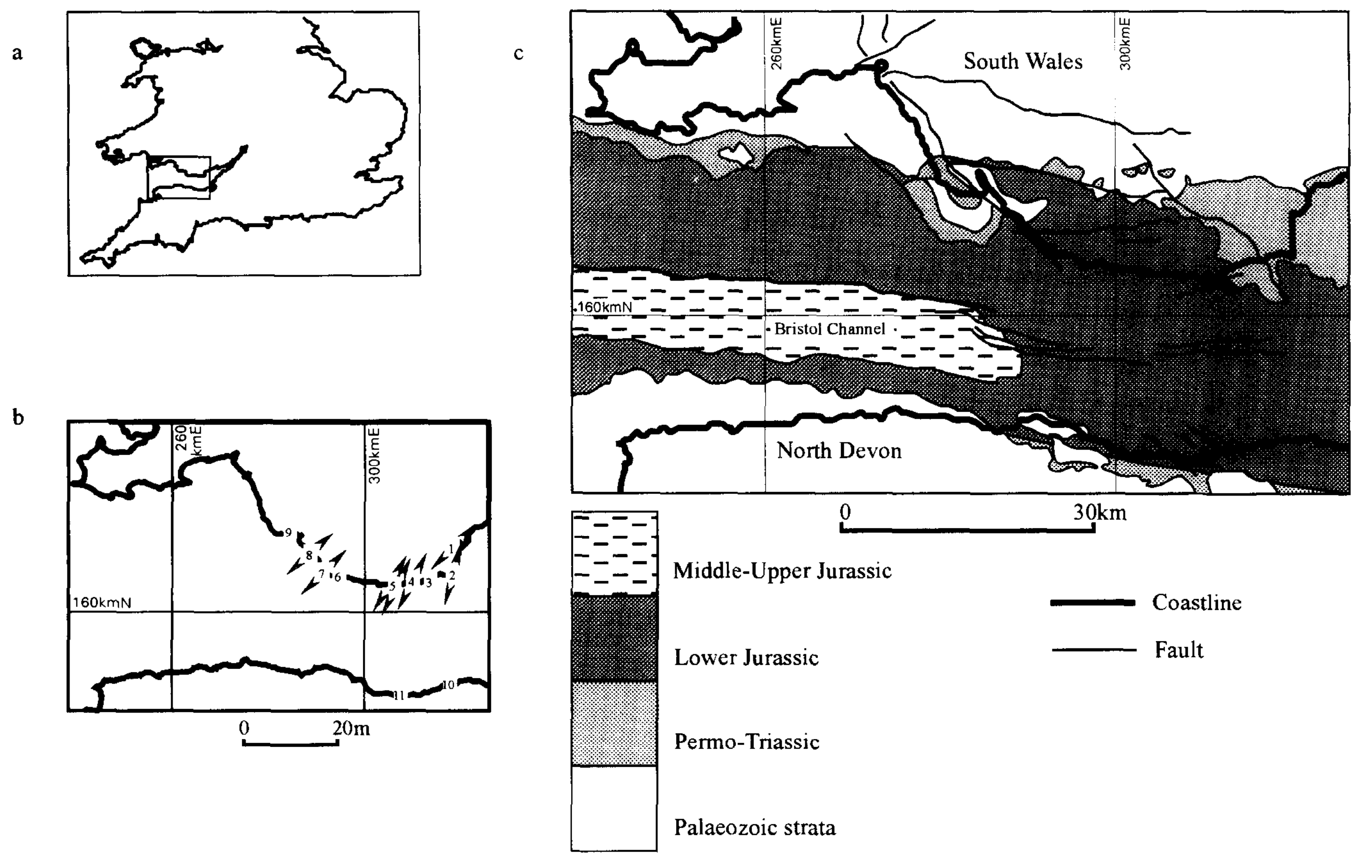

Fig. 1. (a) Map of the southern part of the British Isles showing the area of the inner Bristol Channel studied. (b) Map of the area studied showing the computed σ_3 vectors for the rifting-related extension at the numbered localities. 1 = Penarth marina, 2 = Sully/St Mary's Well Bay, 3 = Bendrick Rock, 4 = Barry Old Harbour, 5 = Rhoose Point, 6 = St Donats, 7 = Nash Point, 8 = Trwyn y Witch/Southerndown, 9 = Sandy Bay, Porthcawl, 10 = St Audrie's Bay, 11 = Watchet. (c) Geological map of the area studied, showing the main faults.

upper 12 m of the Triassic (Rhaetian) section consist of a transgressive unit of marine dark and pale grey mudstones with subordinate sandstones and limestones, that pass upwards into Lower Jurassic marine grey, calcareous mudstones and thin bioclastic calcilutites (Waters *et al.* 1987). A lower Jurassic shoreline facies of conglomerates and calcarenites is locally present along the northern coast of the Bristol Channel. The section is cut by numerous, predominantly WNW–ENE striking normal faults and associated calcite veins, which form the subject of this paper.

FIELD OBSERVATIONS

Figure 2 shows the rift-related macro and meso-scale normal fault populations, most of them developed by brittle faulting, studied in this investigation. Figure 3 shows the associated extensional veins, filled either by idiomorphic calcite crystals or by fibrous calcite oriented normal to the rock walls. Rifting vectors (σ_3), determined from normal faults at localities 1, 2, 4, 5, 7 and 8 (Fig. 1), show a consistent regional pattern. Some of the faults, such as the normal faults at Nash Point (locality 7, Fig. 1), formed above reactivated pre-existing Variscan structures. These faults, with an ENE–WSW strike instead of the typical WNW–ESE strike (Fig. 2), were generated as neoformed oblique-slip normal faults under the regional stress configuration (Fig. 1).

At Rhoose Point (locality 5) two structures, occurring in a region of more dense normal faulting, show Riedel shears and associated extensional veins. The Riedel shears are located in the extensional quadrant, at an angle $\varphi/2$ to the principal displacement zone, where φ is close to 38°—the friction angle in argillaceous calcilutites, determined by Davies *et al.* (1991) from a locality near Gileston between localities 5 and 6 in Fig. 1. These are interpreted as embryonic normal faults, based on the fact that the zone lacks evidence of P and R′ shears, and that the principal displacement zone cuts all the shears. This suggests that the faults present in the outcrop ceased activity at an early stage in their development, as indicated by the shear experiments of Wilcox *et al.* (1973) and Bartlett *et al.* (1981). The structures have been rotated approximately 30° towards the south about an axis parallel to fault strike, in the southern limb of a major roll-over antiform. An array of bed-parallel décollements within mudstone layers has developed within the roll-over, recording layer-parallel displacements. Calcite growth within the décollements took place by a crack-seal mechanism, and shows evidence for multiple reactivations (Fig. 4a). Similar features are also present at Barry Old Harbour (locality 4) in Lower Jurassic rocks.

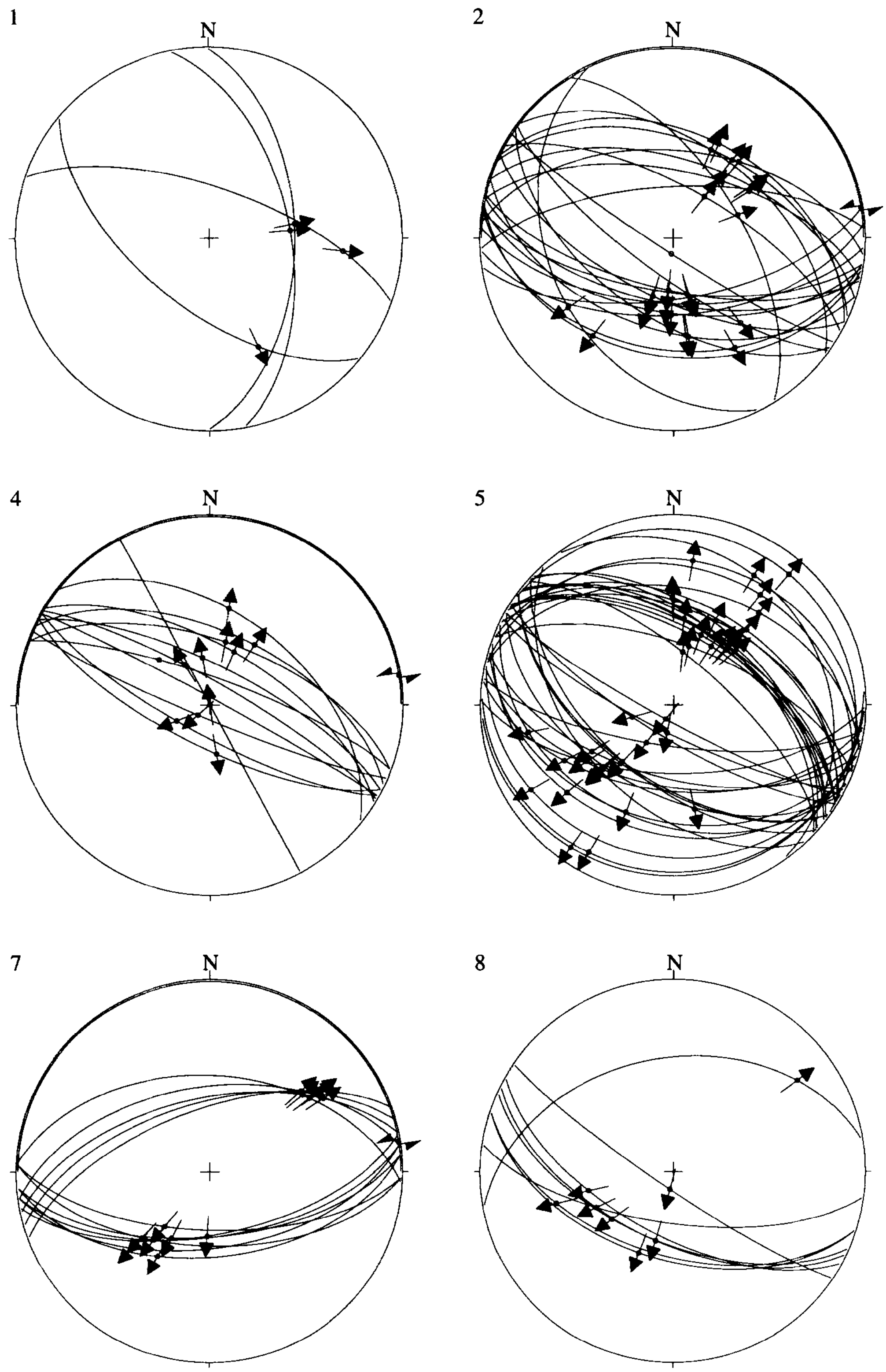

Fig. 2. Rifting-related normal faults shown as great circles on lower hemisphere equal area stereographic projections at the numbered localities (see Fig. 1 for locations). Poles with arrows indicate slip vector in fault plane.

At Watchet (locality 11) two synsedimentary normal faults are present in the Triassic Mercia Mudstone Group. The first of these dips 30° towards 211° in the lower part of its listric shape, and layering in the hangingwall dips 5° to 153°. An undisturbed fissile mudstone bed lies above its upper tip and a sequence of marker beds consisting of three gypsum layers interbedded with siltstone layers show a systematic increase in displacement down the dip of the fault, from 0.15 m in the upper gypsum layer to 1.03 m in the lower gypsum layer. The total thickness of the same stratigraphic section containing the marker beds is 3.7 m in the hangingwall and 3.03 m in the footwall of the fault. The second normal fault dips 20° to 200° and bedding in the

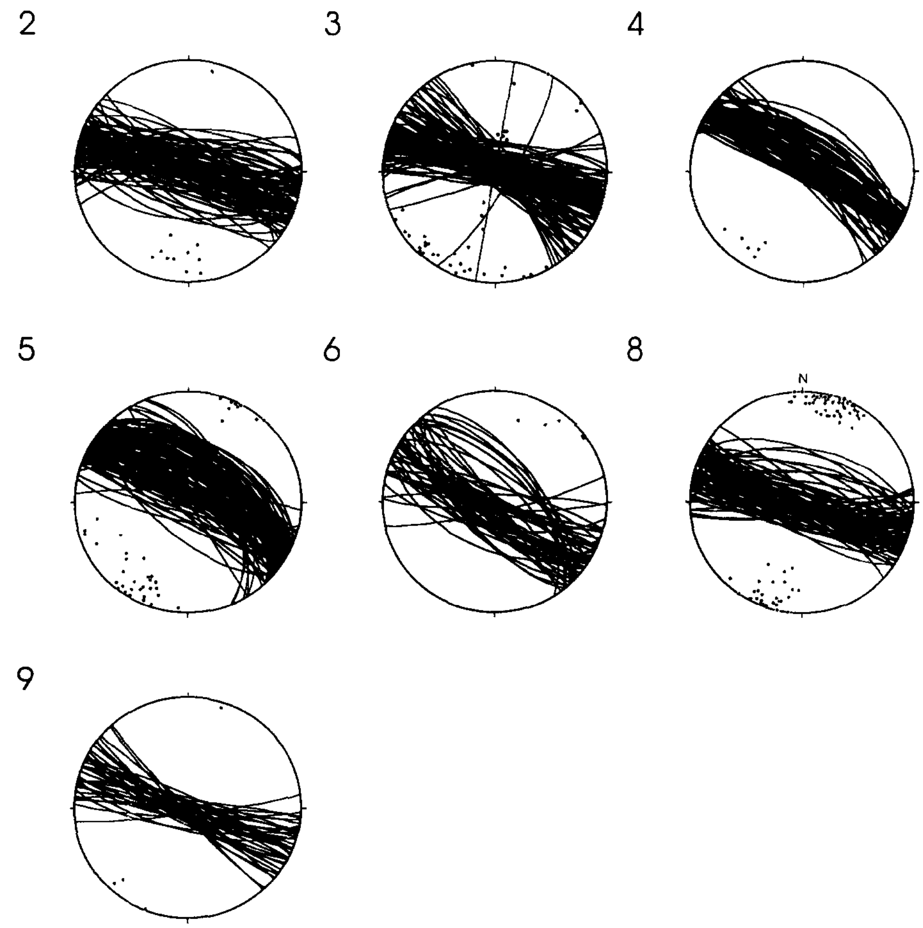

Fig. 3. Rifting-related extensional veins shown as great circles on lower hemisphere equal area stereographic projections at the numbered localities (see Fig. 1 for locations). Poles indicate orientation of mineral fibres in the veins.

hangingwall dips 20° to 049°. In this fault, displaced marker beds indicate dip separations of 0.3 m in the upper portion of the fault, increasing systematically downwards to 1.05 m. The total thickness of the same stratigraphic portions containing the marker beds is 2.59 m in the hangingwall and 2.33 m in the footwall.

Extensional veins are ubiquitously developed in association with the rift related normal faults. The most common mineral filling the veins is calcite. Some of the veins, developed in Triassic and Lower Jurassic sediments, are partly filled by barite, e.g. Barry Old Harbour (locality 4), St Audrie's Bay (locality 10, Fig. 5a), Lavernock Point (to the east of locality 3) (Waters *et al.* 1987), and Ogmore (to the west of locality 8) (Lee 1991). At St Audrie's Bay, on the southern margin of the Bristol Channel, the barite shows growth during early stages of extensional fracturing. Extensional veins in Triassic fissile mudstones commonly contain gypsum in the form of satin spar, that in some cases shows vertical injection structures (e.g. at Penarth Head, to the southeast of locality 1).

Evidence that several deformation mechanisms operated during the rifting event are present. For example, pressure-solution arrays, associated with a shear plane at locality 5, curve from lying perpendicular to σ_1 distant from the shear plane, to sub-parallel slickolitic structures (Hancock 1985) along the shear plane. Many veins are filled by stretched calcite fibres, indicating syn-deformational growth. Evidence for their syn-deformational relationship with normal faulting is present at Rhoose Point and Trwyn-y-Witch (localities 5 and 8), where the veins were formed as pull-aparts, perpendicular to the sub-horizontal layering, and linked by normal faults with slickolites, the likely source of the calcite. This illustrates a typical feature of all the normal faults, in that the fault shear planes change orientation as they pass through differing lithologies. Normal faults occur in mudstone, linked by extensional veins in limestone, indicating contrasting rheological properties for the two lithologies. These veins are often filled by calcite lacking fibrous form. Commonly voids are still present in the veins and are lined by idiomorphic calcite and sometimes barite crystals.

The contrast in rheology of the limestones and mudstones during the extensional deformation is well illustrated in a major normal fault structure at St Audrie's Bay (locality 10). In the downthrown hangingwall of the north-dipping fault, an extensional vein-related boudinage structure has V-shaped clefts that cut through earlier calcite-filled veins (Fig. 5a). The re-opened centres of these veins are filled by barite and calcite, in which the latter is clearly separated from the earlier calcite-fill event. Some of the clefts are filled by an untextured limestone/mudstone mixture derived from

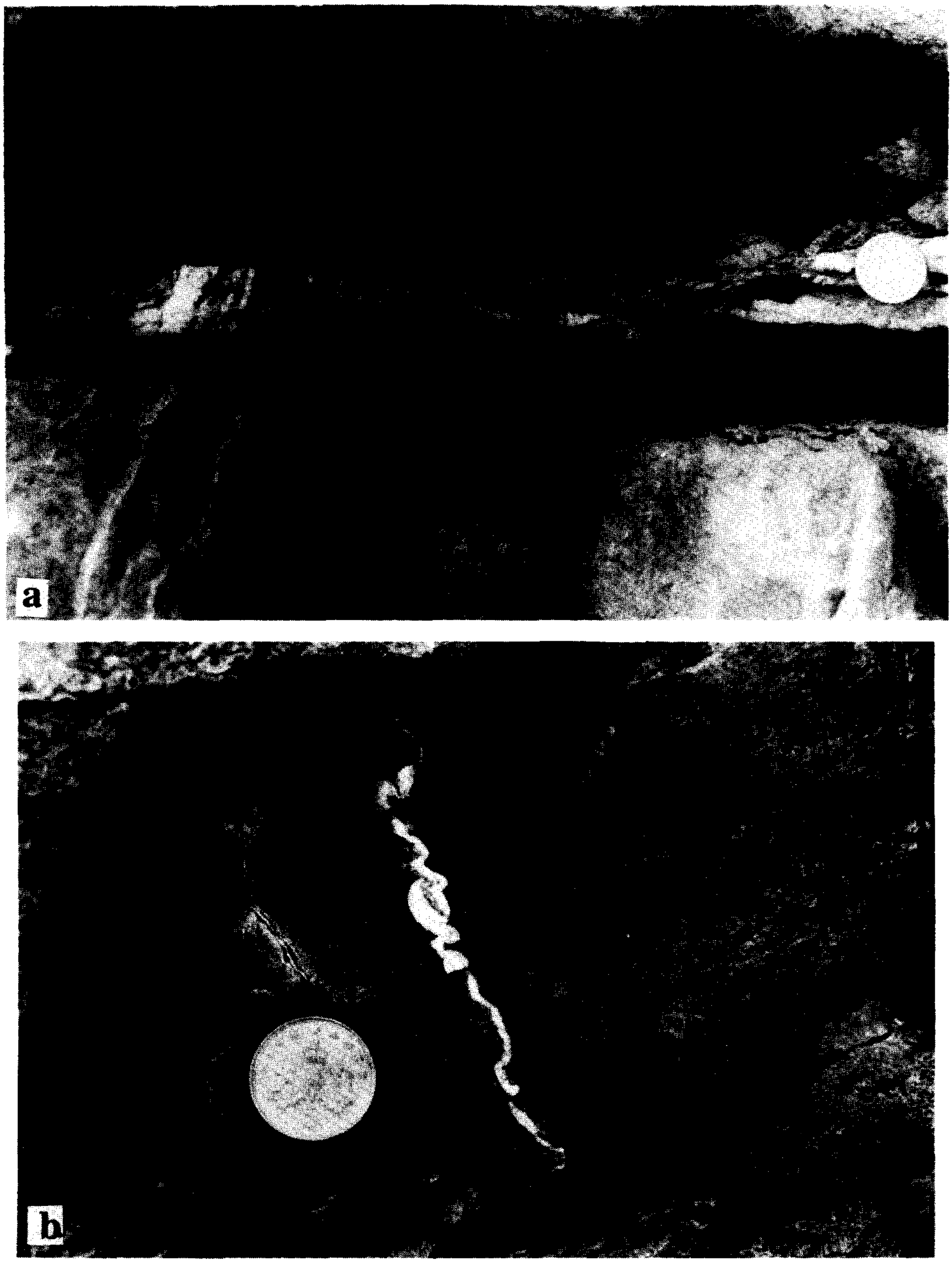

Fig. 4. (a) Calcite filled bed-parallel décollement zone in Lower Jurassic mudstone at Rhoose Point (locality 5, located in Fig. 1). The mineralisation grew by a crack–seal mechanism during the rifting event. (b) Extensional veins at Rhoose Point (locality 5) folded by vertical compaction.

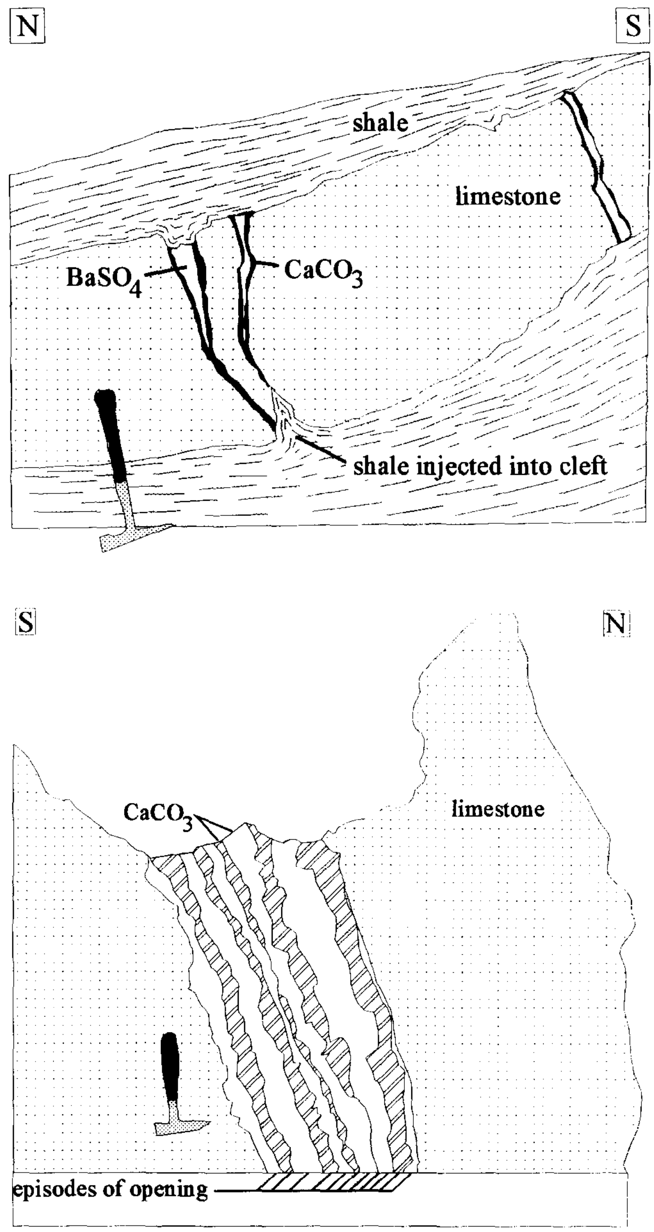

Fig. 5. (a) Shale injections at St Audrie's Bay (locality 10, located in Fig. 1) in Lower Jurassic limestone/mudstone succession. Line tracing shows the limestone layers separated by extensional veins. Internal parts of veins are filled by baryte, external parts by calcite. Clefts formed at tips of veins are filled by injected mudstone. (b) Multiply re-opened extensional calcite veins at Porthcawl (locality 9, located in Fig. 1).

the underlying beds. The normally bed-parallel fabric of the underlying shale is tightly folded into the base of the clefts, suggesting an origin as a soft sediment injection structure, discussed below. The boudinage occurred along discrete minor normal faults. Displacements in the mudstones were so high that these high-angle faults lose their discrete character at the limestone/mudstone boundary. The mudstone layers have accommodated this stretching by ductile deformation, with no discrete shear planes being visible. Differential movement of adjacent mudstone horizons, and movement along brittle fractures in the limestone layers, have produced a significant rotation of the bedding that has in some cases detached lozenge-shaped blocks.

Evidence that extensional veins associated with normal faulting were formed before complete compaction of the sediments is present at Rhoose Point (locality 5). Here, in the footwall of a normal fault, a set of tightly folded, calcite-filled extensional veins is present (Fig. 4b). Their orientation (e.g. 58/90, 04/83, 28/82—dip direction/dip) is similar to that of the other extensional veins in the section (Fig. 3). Their original shape has been folded by compaction that has resulted in a vertical shortening of between 50% and 75%. Bedding planes in the host limestone are irregular, and the limestone is rich in fossils. Similar folded veins have not been observed at any other locality.

Composite, calcite-filled extensional veins are common at localities 4, 5 and 9 (Fig. 5b). Slightly differing forms of the calcite-fill indicate the multi-stage re-opening of the veins.

METHODS AND DATA

Two stages are involved in calculating the stress associated with the extensional faulting in the Bristol Channel. The first is the determination of the orientation of the principal stresses and their ratios, described below. The second involves the determination of stress magnitude, and requires knowledge of the stratigraphic load, and the frictional and cohesive properties of the rocks at the time of their deformation. These parameters, together with the methods for calculating stress magnitude are also discussed below.

It is apparent from extensional veins associated with faults that fluid pressures were important in modifying tectonic stresses in the basin at the time that the extensional faults were active. The nature and origin of these fluids are discussed below.

Calculation of stress orientation and stress ratios

Data from the extensional faults shown in Fig. 2 have been used for a stress inversion calculation. An example of a typical data-set is given in Table 1. Palaeostress configurations under which this, and the fault populations for the other localities, could have originated are listed in Table 2. The stresses have been determined by the grid search routine of Hardcastle & Hills (1991), chosen as one of the numerous currently available palaeostress techniques. Readers are referred to this paper for further details about the algorithm.

Table 1. Data taken from the rifting-related fault population at Trwyn-y-Witch (Fig. 2, locality 8). Each fault datum is characterised by its displacement sense and the confidence level with which the determination was made (1-high, 4-low)

Fault Dip direction	Dip	Slip vector Trend	Plunge	Sense	Confidence
204	60	234	54	Normal	1
206	60	196	59	Normal	1
198	54	256	34	Normal	1
214	83	195	77	Normal	1
209	63	258	48	Normal	1
198	52	202	50	Normal	1
350	40	054	17	Normal	1
188	68	245	52	Normal	1

Data for stress computations

The method used to calculate the magnitudes of the principal stresses, described below, requires knowledge of the stratigraphic load. As the outcrops along the Bristol Channel borders are restricted to the Triassic and Lower Jurassic, it was necessary to estimate the pre-erosional lithostratigraphic column for the area, based on the regional geology (Kamerling 1979, Cope 1984, Cornford 1986, Table 3). Only one set of thickness data is used for all localities for the following reasons: (1) the localities lie in an E–W zone along the Bristol Channel margin, parallel to the presumed lithofacies belts; (2) South Wales is believed to have sourced the Bristol Channel basin during rifting-related pre-Albian deposition; and (3) major normal faults that controlled basin deposition are approximately parallel to the zone of outcrops studied. Any differences in local stratigraphy, not apparent in the generalised column of Table 3 are unlikely to affect the stress magnitude computations more than errors in assumptions made in the algorithm itself.

The additional data required for the stress magnitude computation are rock mechanics parameters. Cohesion and angle of internal friction for both intact and anisotropic rock used in the computation were taken from Davies *et al.* (1991) who analysed samples from a locality near Gileston (between localities 5 and 6 in Fig. 1). Limestone has values for peak and residual cohesion of 29 and 18 MPa respectively, and for peak and residual friction of 38° and 36° respectively. The tensile strength is 25 MPa. Mudstone has peak cohesion and friction of 8 MPa and 25° respectively. Because mudstone fails before limestone, the mudstone values for these rock parameters have been used in the calculation of stress magnitudes for the Triassic and Jurassic through Early Cretaceous rifting events. A Poisson's ratio of 0.344 was used.

The stress magnitude calculations also require data describing porosity and permeability of both the rock and its original sediment (Table 4). Taking into account

Table 2. Palaeostress configurations computed from rifting-related faults at 6 localities shown in Figs. 1 and 2. The orientation of the stress axes is indicated by azimuth/plunge. The stress ratio used is $\phi = (\sigma_2 - \sigma_3)/(\sigma_1 - \sigma_3)$.The BRUTE3 grid search method of Hardcastle & Hills (1991) was used for computation

			Stress tensor			
Locality	Age of rock	No. of faults	Sigma 1	Sigma 2	Sigma 3	Stress ratio
1	Triassic	4	101/70	318/16	225/11	0.2
2	Triassic	18	095/80	285/10	195/02	0.2
4	Lr Jurassic	7	000/80	116/04	207/09	0.1
5	Lr Jurassic	23	051/85	297/02	207/05	0.6
		8	210/70	301/00	031/20	0.9
7	Lr Jurassic	13	045/80	136/00	226/10	0.5
8	Lr Jurassic	7	029/70	137/06	229/19	0.7

Table 3. Estimated pre-erosional lithostratigraphic column for the Bristol Channel borders. Lithological abbreviations: cong = conglomerate, sst = sandstone or sand, mdst = mudstone, cl = clay, sh = shale, lst = limestone, and olst = oolitic limestone. Sources of density data: (1) Brooks, pers. com.; (2) Cain 1982; (3) Briggs 1980; (4) Telford *et al.* (1976); (5) Singh (1976); (6) Brooks & Thompson (1973); (7) Green *et al.* (1965); (8) Kroos *et al.* (1993) and (9) Byerlee (1968). N.B. where no density data are available for a local rock type, data for a similar rock type from the local older sequence have been used, since these will have sourced the Bristol Channel basin-fill. Failing this, data from the literature have been included. In the case of multiple sources, average values (av.) have been used

Age system	Stage	Lithology	Density (kg m^{-3})	Source of density data	Thickness (m)	
					Max	Min
Triassic	Norian–Rhaetian	cong, sst, mdst	2350–2450(2400) (av.)	1,2,4,7	200	—
Lower Jurassic	Hettangian–Toarcian	mdst, lst, sh	2400–2900(2642.6)(av.)	3,4,5,6,7,8,9	800	600
Middle	Bajocian–Bathonian	olst	2400–2550(2475) (av.)	4,7	165	—
Jurassic	Callovian	cl	2210	4	185	145
Upper	Oxfordian	sst	2350	4	260	—
Jurassic	Kimmeridgian	cl	2210	4	165	130
	Portlandian	lst, cl	2380	4	50	-
Cretaceous	Valanginian–Aptian	sst	2350	4	1000	250

that commercial reservoirs have porosities from 10 to 30% and permeabilities of a few millidarcies to 1 darcy (Telford *et al.* 1976), Tables 3 and 4 indicate that the Lower Jurassic sediments behave as seals, and only the overlying portions of the Mesozoic sequence contain sediments that could act as reservoirs.

Table 4. Porosity and permeability data from Triassic and Jurassic rocks used for calculations. Sources of data: (1) Singh (1976); (2) Jaeger & Cook (1976); (3) Matray *et al.* (1993); (4) Kroos *et al.* (1993); (5) Hanebeck *et al.* (1993); (6) Thomas (1962); (7) Houston & Kasim (1982) and (8) Byerlee (1968)

Sediment	Porosity (%)	Permeability (md)	Source
Limestone	0.3–43	< 0.05	2,7,8
Skeletal limestone.	4–15	0.8–25	6
Uncemented Skeletal limestone	19	250	6
Oolitic limestone	0		6
Uncemented Oolitic limestone	15	600	6
Fine grained Limestone	0–3.4		1,6
Sandstone	0.7–34	217	1,2,7
Triassic sandstone	4–22		3
Siltstone	2.2–5.6	< 0.05	1,2
Shale	1.6–25		7
Muddy shale	4.7	< 0.05	2
Source shale	1.66–15		4
Mature silty shale		< 1–2	5
Immature silty Shale		13.2	5

However, studies by many authors (e.g. Robertson 1967, Chilingarian 1983 and Moore 1989) indicate that the sediments acting currently as seals were highly porous and permeable during the time of their deposition. The original sediments underwent two processes: mechanical compaction by fabric rearrangement, plastic deformation and grain breakage; chemical compaction with pressure solution between grains, and various processes of cementation, within the protective and skeletal structures of organisms.

Recent clay and silty sediments have porosities ranging from 65% to over 80% at the time of deposition. However, they progressively undergo compaction of about 50% during burial to a depth of 1 km, when their porosity is about 26% (Kukal 1990 and references therein). Chilingarian (1983) suggested that the initial porosity of clays, of up to 80%, rapidly decreases during the first 500 m of burial. If such a sediment is rich in organic matter, a compaction from 1.4:1 to 30:1 can be expected (Kukal 1990). Moore (1989) described the compaction rate of aragonite mud with an original porosity of 40%. The porosity dropped to 20% and 10% at 400 m and 600 m burial, respectively, which suggests that rapid dewatering occurs. Cementation can begin in the sulphate reduction zone (< 1 m below the sediment/water interface) and continues at the interface between the sulphate reduction zone and the methanogenic zone (< 10 m below the sediment/water interface)

(Bottrell & Raiswell 1990). Bedding-parallel fibrous calcite veins are common in some of the mudstone successions, and these are thought to represent the effects of deeper cementation processes (≈ 500 m depths) probably in the decarboxylation zone (Marshall 1982). More or less complete cementation is likely to have taken place between depths of 600 and 800 m, and the first compaction fracturing occurs at a depth of 1100 m, with a consequent increase in porosity to 30%.

DSDP cores in the areas of recent deposition of carbonate muds document that several million years are sufficient for dissolution of carbonate fossils, complete cementation and recrystallisation (Kukal 1990 and references therein). Bjorkum & Walderhaug (1990) have shown that supersaturation of calcite for cementation is first reached in fossil-rich layers. The nature of the limestone units in the Lower Jurassic limestone/mudstone succession of the Bristol Channel region (Waters *et al.* 1987) suggests that they formed along such fossil-rich layers.

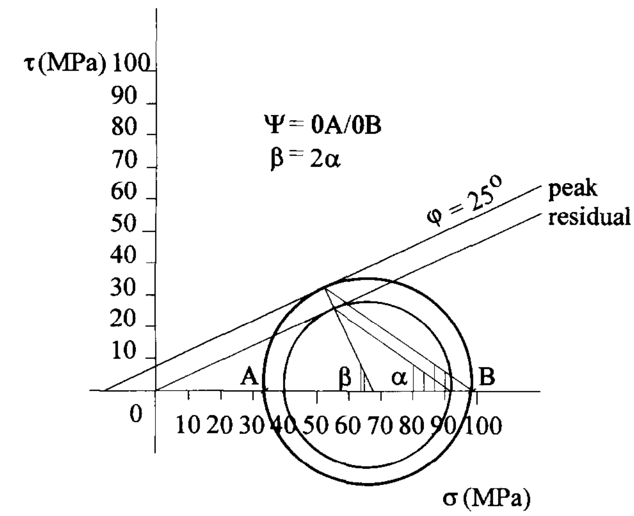

Fig. 6. Mohr envelopes and circles for Lower Jurassic mudstones. Peak values of cohesion and angle of internal friction are 8 MPa and 25° respectively (Davies *et al.* 1991). The value of φ is given by σ_3/σ_1, where σ_3 is distance from origin (O) to A and σ_1 is distance from origin (O) to B. For all stress configurations related to a particular Mohr envelope: α and β angles of all stress states are equal, and $\beta = 2\alpha$.

Stress magnitude computation

The magnitudes of the three principal compressive stresses were calculated using the following equations of Angelier (1989):

$$\psi = \sigma_3/\sigma_1 \qquad (1)$$

$$\phi = (\sigma_2 - \sigma_3)/(\sigma_1 - \sigma_3) \qquad (2)$$

$$\sigma_1 = \sigma_v. \qquad (3)$$

ϕ is the stress ratio, calculated by the stress inversion method, and listed in Table 2.

For a given lithology, the ratio of minimum to maximum principal stress (φ) is derived from the Mohr circle and envelope construction shown in Fig. 6. The Mohr envelope is first constructed as a line inclined to the x-axis (normal stress) at the angle of internal friction φ (Fig. 6), and cutting the y-axis (shear stress) at the value of cohesion. An arbitrary Mohr circle is then constructed tangentially to the envelope, giving a value for the angle β or α ($\beta = 2\alpha$, Fig. 6). For normal faulting, the value for σ_1 equals the overburden load σ_v, which is given by ρgh, where ρ is the density, g the acceleration of gravity (rounded to 9.812 ms^{-2}), and h the thickness of overburden. Knowing σ_1 and the angle α, σ_3 is found by the Mohr circle construction, and the value of φ can then be calculated using equation (1).

Finally σ_2 can be calculated by combining equations (1)–(3):

$$\sigma_2 = \sigma_v(\phi + \psi - \phi\psi). \qquad (4)$$

Two methods have been used to determine the overburden load σ_v. In the case of synsedimentary faulting, such as the normal faulting at Watchet (locality 11), an arbitrary value of 50 m for the burial depth has been assumed. The density of the uncompacted overlying sediment is derived from the rock density, the initial sediment porosity and the density of the pore fluid (assumed to be water with a density of 1000 kg m^{-3}).

Where no evidence for synsedimentary faulting is present, faulting could have occurred at any stage between the Norian and Aptian, and thus at various burial depths. In this case a range of tectonic stress configurations is computed assuming different values of overburden load σ_v. Table 5 lists six cases for burial depths of 100, 200, 300, 400, 600 and 800 m.

Modelling of tectonic stresses at various overburden states

Taking into account the observed soft sediment faulting, any one of these six cases could represent the values for the tectonic stresses developed in the basin during the rifting event. In each case any subsequent faulting event will have occurred under an increased overburden load, adding to the tectonic stress and resulting in a decreased stress ratio. Figure 7 shows the effect of addition of overburden to the tectonic stress of case 2 (initial faulting in Lower Jurassic rocks at 200 m burial) in 11 steps until the end of the Lower Cretaceous,

Table 5. Values of stress magnitudes calculated for the stress ratio $\phi = (\sigma_2 - \sigma_3)/(\sigma_1 - \sigma_3) = 0.9$, and different values of burial in the Lower Jurassic succession. Assumed rock and water densities were 2642.6 and 1000 kg m^{-3}; cases 1, 2 and 3 assumed 40% porosity, and 100, 200 and 300 m burial, respectively; case 4 assumed 20% porosity and 400 m burial; and cases 5 and 6 assumed 10% porosity and 600 m and 800 m burial respectively

	σ_1	σ_2	σ_3	$\psi(\sigma_3/\sigma_1)$
Case 1	1.95 MPa	1.79 MPa	0.15 MPa	0.08
Case 2	3.90 MPa	3.66 MPa	1.57 MPa	0.40
Case 3	5.84 MPa	5.53 MPa	2.72 MPa	0.47
Case 4	8.11 MPa	7.89 MPa	4.91 MPa	0.60
Case 5	12.98 MPa	12.56 MPa	8.80 MPa	0.68
Case 6	17.84 MPa	17.31 MPa	12.53 MPa	0.70

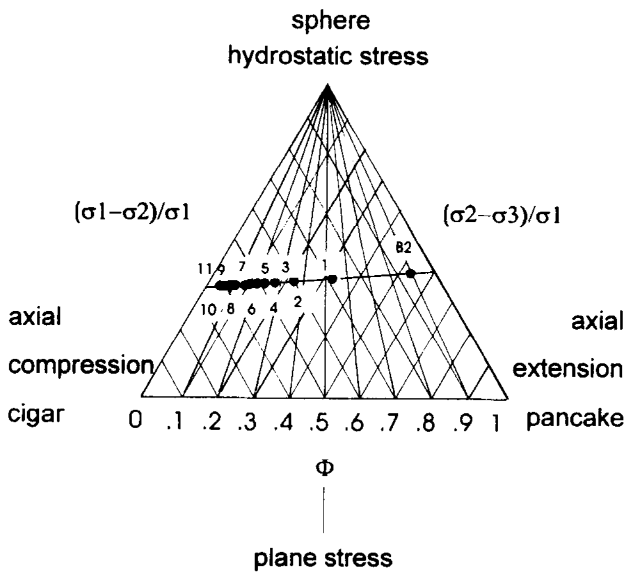

Fig. 7. Triangular diagram representing the shapes of stress ellipsoids, plotting $(\sigma_1-\sigma_2)$ and $(\sigma_2-\sigma_3)$, both normalised with respect to σ_1, along the left and right hand axes respectively. The ratio of the principal stresses $\phi=(\sigma_2-\sigma_3)/(\sigma_1-\sigma_3)$ is plotted along the horizontal axis. All ellipsoids lying along a line radiating from the upper apex have the same stress ratio, indicated by the intersection of the line with the horizontal axis. See Nemcok (1995) for a detailed explanation. The diagram shows the stress ratios (ϕ) of the stress configuration resulting from the addition of overburden to the tectonic stress for case 2 (B2) from Table 5. Points 1–6 indicate the results after additional 100, 200, 300, 400, 500, 600 m of Lower Jurassic succession; points 7–11 indicate the results calculated for the Middle Jurassic, and the Middle/Upper Jurassic (Oxfordian/Kimmeridgian), the Jurassic/Cretaceous and the Lower/Upper Cretaceous boundaries. Poisson's ratio $n=0.344$, and density values from Table 3 have been used.

when rifting is thought to have ceased. The stress ratio progressively decreases from its original value of 0.9, at the time when 200 m of Lower Jurassic sediments had been deposited, to the value 0.05 at the Aptian/Albian boundary. Increments of vertical load were added directly to the σ_1 value. The consequent increases in the σ_2 and σ_3 stresses are given by $\upsilon/(\rho g h(1-\upsilon))$ following Jaeger & Cook (1976), where υ is Poisson's ratio, ρ density, g acceleration due to gravity and h thickness.

Origin and character of water in the sedimentary sequence

The major fluid phase is provided by depositional water. By analogy with Upper Triassic waters in the Paris Basin (Matray *et al.* 1993), it is likely that the Triassic (Norian) succession of the Bristol Channel region contained Na–Ca–Cl type waters with a high saline load. In the Paris Basin, concentrations of Ca are higher than values expected for NaCl secondary brines. Matray *et al.* (1993) suggested that Ca enrichment took place during the formation of brines and their long-range transport through Upper Triassic layers. The Lower Jurassic sequence will also have trapped its own water.

However, only part of the water volume will have been provided by fluids trapped during deposition. It is likely that an additional proportion of Upper Triassic waters was formed by the following reaction, suggested by Worden & Smalley (1993):

$$CaSO_4 + CH_4 \rightarrow CaCO_3 + H_2S + H_2O$$

$$Mg^{2+} + CaSO_4 \rightarrow Ca^{2+} + MgSO_4.$$

Both reactions are therefore very likely since methane could be provided by maturation of the Lower Jurassic source rocks, and calcium sulphate by solution of Triassic gypsum. Recent outcrops of Upper Triassic show evidence of solution of gypsum horizons. The first reaction might have been active later, when the younger Lower Jurassic source rocks started to produce hydrocarbons, which would require a significant amount of overburden. Such an increased depth would agree with the fact that this reaction has an autocatalytic character with increased temperature (Worden & Smalley 1993). However, in the Wessex Basin the Lower Jurassic source mudstones produced type II kerogen (Stoneley & Selley 1986), which generates predominantly oil with only minor quantities of gas (Leythaeuser 1993). Since all the hydrocarbons would have been expelled as a single phase fluid, maturation and expulsion will not have generated sufficient methane for reaction 2 to proceed to any significant extent. However, the experimental work of Kroos *et al.* (1993) suggests that this expulsion will itself have produced a large amount of water and additional pore space at the maturity level for the region determined by Cornford (1986).

Jenkins & Senior (1991) analysed the $^{18}O/^{13}C$ isotopic composition of water in both the Toarcian fill of synsedimentary dykes and the fibrous calcite of some of the synsedimentary fractures. The water of the dyke fill indicated a marine origin, whereas that of the fibrous calcite from the upper levels of the fractures suggested fresher water derived from underlying Lower Jurassic organic rich clays. However, as pointed out by Chilingarian (1983), the salinity of solutions squeezed out from mudstones progressively decreases with increasing overburden pressure, and can become fresher than water in sandstones and limestones belonging to the same sequence.

RESULTS AND INTERPRETATION

Tectonic stresses during the Triassic and Jurassic through Early Cretaceous rifting events

The calculated σ_3 orientations for the Triassic rocks at Penarth and Sully/St Mary's Well Bay (localities 1 and 2) are similar to those at the other localities along the northern coast of the Bristol Channel (Table 2 and Fig. 1). Most of the faults were formed in at least partly lithified rocks by brittle faulting. The only synsedimentary normal faulting was observed in the sediments of the Triassic Mercia Mudstone Group at Watchet (locality 11). The tectonic stresses can be calculated directly for localities 1 and 2 using the first method described above. By assuming a burial depth of 50 m at the time of faulting, and with average densities for rock and water of 2400 kg m^{-3}, and 1000 kg m^{-3} respectively and a porosity of 67.5%, and using $\phi = 0.2$ (Table 2), the calculation yields $\sigma_1 = 0.714$ MPa, $\sigma_2 = 0.169$ MPa and $\sigma_3 = 0.033$ MPa. If additional overburden is added to this Triassic tectonic stress, which has a ratio of $\phi = 0.2$, the resulting stress configuration would decrease the ratio. However, the stress ratios calculated for the Lower Jurassic localities listed in Table 3 show values equal to, or higher than, plane stress ($\phi = 0.5$). The only exception is Barry (locality 4) with $\phi = 0.1$. Thus, most of the Lower Jurassic localities indicate stress configurations with extension playing a significant role, and none of them could be explained by simple addition of overburden to the stress computed for synsedimentary Triassic faulting.

It is possible to establish which of the six tested Lower Jurassic stress configurations approximates to the tectonic stress field, using the following technique. There is field evidence for a protracted period of rifting until the end of the Aptian (Cornford 1986, Stoneley & Selley 1986, Roberts 1989, Jenkins & Senior 1991). The Bristol Channel Lower Jurassic localities show a range of stress ratios from 0.1 to 0.9, computed by inversion stress methods (Table 2). However, it is likely that the tectonic stress configuration that caused rifting would have been very prolate (strongly extensional), with a stress ratio of about 0.9. Thus the stress configurations that controlled the faulting at the different Lower Jurassic localities have been modified by an increased σ_v, caused by additional overburden. This implies that the faulting at the different localities occurred during different younger episodes between the Lower Jurassic and Lower Cretaceous,

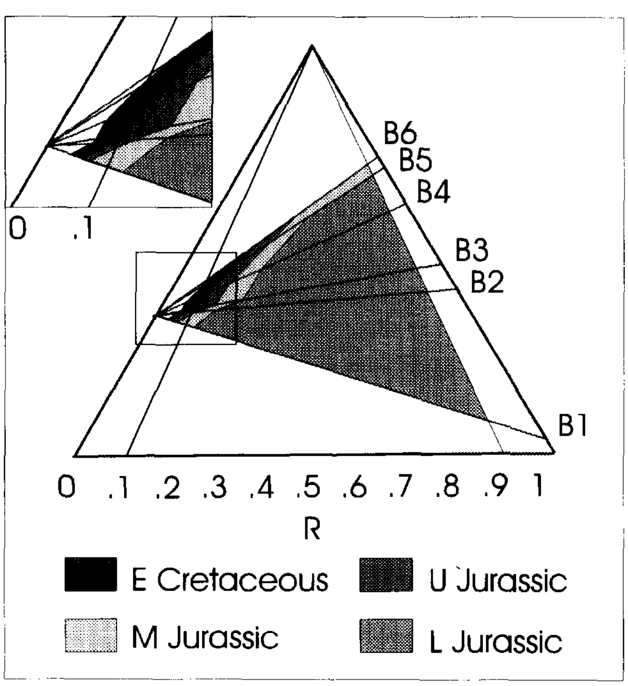

Fig. 8. Triangle diagram (for explanation of diagram see caption to Fig. 7 (Nemcok 1995)) showing the stress ratios of stress configurations resulting from the addition of overburden to the tectonic stress of the 6 cases from Table 5 (B1–B6). Procedure as in Fig. 7. The inset shows an enlargement of the region of minimum stress ratios for each case. Cases 1–4 result in a minimum stress ratio less than 0.1, and case 6 in a minimum stress ratio greater than 0.1. Case 5 results in a stress ratio close to the observed minimum of 0.1.

resulting in progressively smaller stress ratios, with a minimum of 0.1 (Table 2). Figure 8 shows the results of incremental overburden addition to each of the six possible 'tectonic' stresses given in Table 5 for the time steps between the age of the tested tectonic stress and the Aptian/Albian boundary. The youngest configurations of cases 1–4 and 6 are either smaller or larger, respectively, than the 0.1 limit. The best fit, given by case 5, indicates both the level of tectonic stress, and the age that this rifting event started, i.e. after 600 m of Lower Jurassic limestone and mudstone had been deposited, towards the end of the Pliensbachian. Our data reveal a significant interval in the faulting between the Triassic and end Lower Jurassic, followed by a succession of fault events through to the Early Cretaceous. The end Lower Jurassic stress magnitudes, $\sigma_1 = 12.98$ MPa, $\sigma_2 = 12.56$ MPa and $\sigma_3 = 8.80$ MPa, show a major change in stress configuration from the earlier Triassic event. This may represent the onset of rifting, with earlier stages showing a prolate character of the stress ellipsoid and later stages with an oblate stress ellipsoid.

Extensional veins–fluid pressure cyclicity

The occurrence at Rhoose (locality 5) of compaction folded, calcite-filled extensional veins vertically shortened by 50–74% (Fig. 4b), indicates that the extensional veins originated during the early stages of burial. There is clear evidence that these veins were associated with the normal faulting in the area, and thus the end Lower Jurassic age of faulting deduced in the previous section appears to be at variance with the partially compacted state of the Lower Jurassic sediments. The paradox can be explained by invoking overpressured pore fluids, as discussed below, which prevented the normal processes of compaction until fault-induced fractures allowed the fluid to escape.

Moore (1989) has shown that freshly deposited mud-supported shelf sediment (wackestone) has a porosity of about 60–78%. An apparently stable grain framework is reached for this type of sediment at approximately 40% porosity under a burial of 100 m or less (Moore 1989). This is the stage when grain-to-grain contact is reached after an average of 61% of vertical shortening has been recorded. We presume that the state of apparently stable grain framework represents a threshold for the development of our extensional veins. However, a vertical shortening of only 60% would reduce sediment porosity from 40% to zero. This type of fully lithified sediment has a porosity of 0.3–5% (Table 4), requiring an even lower amount of compaction. However, as suggested earlier, irregular bedding planes recorded at Rhoose indicate differential compaction, that could explain localised higher values of compaction calculated at this locality. It should be stressed that no similarly compacted veins have been found at other localities, suggesting unique conditions preventing compaction occurred at locality 5, Rhoose.

Other, uncompacted, extensional veins are either filled by fibrous calcite or both idiomorphic calcite and barite.

They have been formed as sediments, undergoing diagenesis, progressively increased in cohesion, shear strength and Poisson's ratio.

The fibrous extensional veins can be explained as crack-seal growth synchronous with their opening. They formed when fluids became available as a result of: (1) expulsion from the sediment by compaction; (2) hydrocarbon expulsion; (3) dissolution of gypsum; or (4) pressure solution induced by the stress concentration at the tips of elastically opened fractures.

The extensional veins that lack a fibrous fill occurred where fractures opened faster than the rate of fluid supply. Veins containing idiomorphic crystals indicate the presence of hydrocarbons in the system which prevented the fractures being fully sealed by precipitation from the migrating fluids. Some of the calcite will have been derived locally from dissolution of fossils, a process that started during the initial stages of diagenesis (Bjorkum & Walderhaug 1990). Barite on the other hand indicates long-range fluid migration. The occurrence of soft sediment injections into extensional fractures at St Audrie's Bay (locality 10) indicates that these structures formed during the early stages of diagenesis. At that time, the limestones were nearly lithified, cemented by calcite in part provided by fossil-rich layers in the mudstone sequence. Their cementation caused an abrupt loss of porosity, when they will have acted as hydraulic seals between unlithified mudstones. The soft sediment injections were caused by overpressuring within the shale layers. The fluid overpressure was caused by the increasing overburden (i.e. compaction), and by the input of additional water into the system, resulting from hydrocarbon expulsion or gypsum dissolution.

The presence of overpressured units suggests that the assumptions made in the calculation of the magnitudes of tectonic stresses were too simplified. The evidence of overpressuring implies that the Lower Jurassic succession was not normally compacted, because the load of overburden was largely borne by the pore fluids rather than by the sedimentary particles. This would slow down the effects of diagenesis.

The numerous fault-related composite extensional veins (Fig. 5b), indicate many episodes of re-opening, and suggest a cyclicity in the development of the overpressuring. Each build-up was caused by a local acceleration of deposition in a normal-fault related system. Fluid pressure increased from its hydrostatic levels towards the lithostatic value. The magnitudes of the regional tectonic stresses were reduced by the fluid pressure to the levels of effective stresses. It caused a shift of the reduced Mohr circle along the x-axis towards the origin until fracturing occurred. As shown in Fig. 6, the situation changed after the first cycle, when, once failed, cohesion and the angle of internal friction decrease from their peak values for intact rock, to their residual values. Each fracture event resulted in fluid discharge from the overpressured zones along the normal faults. After each discharge, the level of fluid pressure returned to hydrostatic value and mineral precipitation commenced within the fractures. Mineral precipitation laterally sealed the unlithified layers and allowed fluid pressure to build-up, thus starting a new cycle.

The juxtaposition of extensional veins in limestone and normal faults in mudstone indicates a drop in effective stresses and a shift of the Mohr circle to the left. Rock strength testing suggests that the compressional strength of a rock is greater than its shear strength, which in turn is greater than its tensional strength. Each of these strength parameters is greater for a limestone than for a mudstone. Thus, as fluid pressures increased, so the magnitudes of the principal stresses decreased until they reached a value when shear failure occurred in mudstone, but only extensional failure was possible in limestone.

DISCUSSION

Additional factors influencing the stress analysis

The principal objective of this paper is to demonstrate how stress magnitude calculations can be used to identify distinct rifting events. In order to clarify the procedure, some simplifying assumptions have been introduced into the calculations. Although these modify the final results, they do not seriously affect the overall technique.

The first simplifications were made in the computation of the six tectonic stresses in Table 5. In order to calculate the overburden stress (σ_v) a fixed sediment porosity for each of the chosen depth intervals was assumed. In reality the amount of compaction within these 100 and 200 m intervals would differ. For example, the equation:

$$e = e_1 - b.\log D, \tag{5}$$

where e is the void ratio at burial depth D, e_1 is the void ratio at a depth of 1 m, and b is the compressibility of clay, was derived for the void ratio in Lower Jurassic mudstones of NW Germany (Chilingarian 1983).

The function will be even more complex if we take into account diagenetic factors other than compaction. For example, Moore (1989) has shown how cementation and dissolution influence porosity with depth. In the case demonstrated by Moore (1989) during the first 450 m of burial, the mudstones increase in cementation from 5 to 20%. Dissolution increases during the same interval from 20 to 30%, but then finally drops to 20%. During the subsequent 450–600 m depth interval, the dominance of these two factors interchanges. Dissolution decreases from 20 to 10% whilst cementation remains the same. Mudstone experiences peak cementation from 20 to 45% in the 600–800 m depth interval. These effects would modify the estimates we have used for sediment densities.

A further simplification was made by ignoring the consequences of effective stress. The real overburden stress should be calculated as:

$$\sigma_e = \sigma_v - p, \tag{6}$$

where the effective load (σ_e) equals the total vertical load (σ_v), used in our simplified approach, minus the pore fluid pressure (p).

Effective stress also influences estimates of the overburden load added to the tectonic stresses at various depths, in the construction of Figs. 7 and 8, where the total vertical load, instead of the effective load, was added to the tectonic stress. Another simplification concerns the use of a fixed Poisson's ratio (υ). In reality, increasing effective overburden increases the various rock properties such as cohesion and Poisson's ratio (υ), which should change as a function of all factors mentioned in the earlier parts of this discussion.

The field work has shown that the lithologies of the Lower Jurassic limestone/mudstone succession have resulted partly from diagenesis. The evidence suggests, in agreement with previous workers (Hallam 1964, Wobber 1965, Weedon & Jenkyns 1990), that the original sediment had a non-uniform character, with its framework apparently controlled by input of material into a shelf environment. The present succession shows a differential compaction related to a varying percentage of mud in the sediment. Chilingarian (1983) has shown that skeletal carbonates undergo greater compaction than mudstone, which accords with our observations. This evidence would imply a lateral variation in the effective overburden.

However, the main factor influencing a non-uniform distribution of overburden would have been local fault-controlled subsidence and deposition, which should also be incorporated into the analysis.

Role of the fluid pressure

Our study has shown a cyclic behaviour in the fluid pressure. This was the third major factor, in addition to overburden and tectonic stress, that controlled the normal faulting and extensional fracturing.

Equation (6) shows that the total load σ_v is supported jointly by the fluid and rock material. The effective stress σ_e is the stress borne by the rock grains. As the limestone layers developed inside the Lower Jurassic succession during diagenesis, their porosity was reduced and they started to act as hydraulic seals. Mudstone horizons would thus experience an increase in fluid pressure above the hydrostatic value. Rocks would fracture when potential normal fault planes undergo a shear stress τ obeying Coulomb's equation:

$$\tau \geq c + (\mu\sigma_n - p) \tag{7}$$

where c is the shear strength of the rock, μ internal friction, σ_n normal stress and p fluid pressure. The newly formed fracture zones will immediately allow fluid to drain from the overpressured mudstone layers. After the first episode of normal faulting, the fracture zones will become sealed by minerals precipitating from the migrating fluids, and a new cycle of overpressuring will start. This fluid pressure cyclicity would further complicate the calculations.

The fluid pressure cyclicity would itself delay the diagenetic processes, and result in the estimated porosity being reached at a greater depth and at a later period than predicted. This implies that the onset of the second rifting period was later than suggested by the modelling shown in Fig. 8.

CONCLUSIONS

(1) Palaeostress analysis of faults and extensional veins in the Mesozoic Bristol Channel basin indicate the operation of a stress system with σ_3 oriented NE–SW and a range of stress ratios $((\sigma_2 - \sigma_3)/(\sigma_1 - \sigma_3))$ from 0.9–0.1. Growth faulting and soft sediment deformation, present both within the Bristol Channel area and in areas to the east, suggest that rifting occurred periodically from Triassic to Early Cretaceous.

(2) Two methods for calculating the magnitudes of the tectonic stresses are discussed, using the equations of Angelier (1989) and Mohr circle and envelope constructions. The first involves data from synsedimentary faults, and yields, for Triassic rifting, $\sigma_1 = 0.714$ MPa, $\sigma_2 = 0.147$ MPa and $\sigma_3 = 0.033$ MPa. The second is developed for faulting in the Lower Jurassic succession, where no direct evidence of age is available, and uses an iterative process of burial load addition to determine the age of faulting that reproduces most closely the calculated range of stress ratios. The results indicate that the faulting is likely to be of end Early Jurassic age (after 600 m of Lower Jurassic deposition) with principal stress magnitudes of $\sigma_1 = 12.98$ MPa, $\sigma_2 = 9.18$ MPa, $\sigma_3 = 8.80$ MPa.

(3) Compacted, calcite-filled extensional veins, associated with normal faulting in Lower Jurassic rocks, indicate that these sediments were prevented from normal compaction by fluid overpressure until the end Early Jurassic rifting opened fractures that allowed fluid escape.

(4) The methods developed employ several simplifying assumptions, which, although not affecting the principle of the methods, could be refined to produce more realistic results. These involve: varying the load with time according to changing compaction and diagenesis; considering the effect of fluid pressure; and taking into account variations in far-field tectonic stresses.

Acknowledgements—This research was undertaken whilst MN was a Royal Society Research Fellow at University of Wales Cardiff. Funds for fieldwork were made available by the University of Wales Cardiff. RAG wishes to thank John Underhill for help in earlier fieldwork and valuable discussion. MN is grateful to Don Secor for introducing him to the theory of hydrofracturing. Richard Lisle, Sara Vandycke, and Mike Brooks contributed helpful advice and discussion. The final version of the paper was greatly improved by constructive criticism from Paul Hancock, Joe MacQuaker and a third anonymous referee.

REFERENCES

Angelier, J. 1989. From orientation to magnitudes in paleostress determinations using fault slip data. *J. Struct. Geol.* **11**, 37–50.

Bartlett, W. L., Friedman, M. & Logan, J. M. 1981. Experimental folding and faulting of rock under confining pressure. Part IX: wrench faults in limestone layers. *Tectonophysics* **79**, 255–277.

Bjorkum, P. A. & Walderhaug, O. 1990. Geometrical arrangement of calcite cementation within shallow marine sandstones. *Earth Sci. Rev.* **29**, 145–161.

Bottrell, S. & Raiswell, R. 1990. Primary versus diagenetic origin of Blue Lias rhythms (Dorset, U.K.): evidence from sulphur geochemistry. *Terra Nova* **1**, 451–456.

Briggs, D. J. 1980. An investigation into variations in mineralogical and mechanical properties of coal measure strata. Unpublished Ph.D. Thesis, University of Wales, Cardiff.

Brooks, M. & Thompson, M. S. 1973. The geological interpretation of a gravity survey of the Bristol Channel. *J. geol. Soc. Lond.* **129**, 245–274.

Brooks, M., Trayner, P. M. & Trimble, T. J. 1988. Mesozoic reactivation of Variscan thrusting in the Bristol Channel area, U.K. *J. geol. Soc. London* **145**, 439–444.

Byerlee, J. D. 1968. Brittle–ductile transition in rocks. *J. geophys. Res.* **73**, 4741–4750.

Cain, P. R. M. 1982. An examination of permanent roadway support design and its relation to proximate geology. Unpublished Ph.D. Thesis, University of Wales, Cardiff.

Chadwick, R. A. 1986. Extensional tectonics in the Wessex Basin, southern England. *J. geol. Soc. Lond.* **143**, 465–488.

Chadwick, R. A. & Smith, N. J. P. 1988. Evidence of negative structural inversion beneath central England from new seismic reflection data. *J. geol. Soc. Lond.* **145**, 519–522.

Chilingarian, G. V. 1983. Compactional Diagenesis. In *Sediment Diagenesis* (edited by Parker, A. & Sellwood, B. W.) D. Reidel Publishing Company.

Cope, J. C. W. 1984. The Mesozoic history of Wales. *Proc. geol. Ass.* **95**, 373–385.

Cornford, C. 1986. The Bristol Channel Graben: organic geochemical limits on subsidence and speculation on the origin of inversion. *Proc. Ussher Soc.* **6**, 360–367.

Davies, P., Williams, A. T. & Bomboe, P. 1991. Numerical modelling of Lower Lias rock failures in the coastal cliffs of South Wales. In: *Coastal Sediments '91* (edited by Kraus, N. C., Ginger-Ich, K. J. and Kriebel, D. J.) Am. Soc. Civ. Eng., New York, 1599–1612.

Green, G. W., Welch, F. B. A., Kellaway, G. A., Ponsford, R. A., Brooks, M. & Mitchell, M. 1965. *Geology of the Country around Wells and Cheddar*. Memoirs of the Geol. Surv. of Great Britain, London.

Hallam, A. 1964. Origin of the limestone–shale rhythm in the Blue Lias of England: a composite theory. *J. Geol.* **72**, 157–169.

Hancock, P. L. 1985. Brittle microtectonics: principles and practice. *J. Struct. Geol.* **7**, 437–457.

Hanebeck, D., Kroos, B. M. & Leythaeuser, D. 1993. Experimental investigation of petroleum generation and migration under elevated pressure and temperature conditions. In: *Geofluids '93, Contributions to an International Conference on Fluid Evolution, Migration and Interaction in Rocks* (edited by Parnell, J., Ruffell, A. H. & Moles, N. R.). British Gas, ext. abs.

Hardcastle, K. C. & Hills, L. S. 1991. BRUTE3 and SELECT: Quickbasic 4 programs for determination of stress tensor configurations and separation of heterogeneous populations of fault-slip data. *Comput. Geosci.* **17**, 23–43.

Houston, W. N. & Kasim, A. G. 1982. Physical properties of porous geologic materials. *Spec. Publs. geol. Soc. Am.* **189**, 143–162.

Jaeger, J. C. & Cook, N. G. W. 1976. *Fundamentals of rock mechanics*. J. Wiley and Sons, New York.

Jenkins, H. C. & Senior, J. R. 1991. Geological evidence for Intra-Jurassic faulting in the Wessex Basin and its margins. *J. geol. Soc. Lond.* **148**, 245–260.

Kamerling, P. 1979. The geology and hydrocarbon habitat of the Bristol Channel Basin. *J. Petrol. Geol.* **2**, 75–93.

Kroos, B. M., Leythaeuser, D. & Hanebeck, D. 1993. Volume balance of a maturity sequence of the Lower Jurassic Toarcian (Lias E) source rock reflects progress of petroleum generation/expulsion. In: *Geofluids '93, Contributions to an International Conference on Fluid Evolution, Migration and Interaction in Rocks* (edited by Parnell, J., Ruffell, A. H. & Moles, N. R.) British Gas, ext. abs.

Kukal, Z. 1990. The rate of geological processes. *Earth Sci. Rev.* **28**, 1–284.

Lake, S. D. & Karner, G. D. 1987. The structure and evolution of the Wessex Basin, southern England: an example of inversion tectonics. *Tectonophysics* **137**, 347–378.

Lee, C. W. 1991. Baryte and calcite cements in the 'breccias' of Ogmore-by-Sea, South Wales. *Geology Today* **7**, 133–136.

Leythaeuser, D. 1993. Petroleum generation and expulsion. In: *Geofluids '93, Contributions to an International Conference on Fluid Evolution, Migration and Interaction in Rocks* (edited by Parnell, J., Ruffell, A. H. & Moles, N. R.) British Gas, ext. abs.

Marshall, J. D. 1982. Isotopic composition of displacive fibrous calcite veins: reversals in pore water composition trends during burial diagenesis. *J. sedim. Petrol.* **52**, 615–630.

Matray, J. M., Fouillac, C. & Worden, R. H. 1993. Thermodynamic control on the chemical composition of fluids from the Keuper aquifer of the Paris Basin. In: *Geofluids '93, Contributions to an International Conference on Fluid Evolution, Migration and Interaction in Rocks* (edited by Parnell, J., Ruffell, A. H. & Moles, N. R.) British Gas, ext. abs.

Moore, C. H. 1989. *Carbonate Diagenesis and Porosity*. Developments in Sedimentology 46, Elsevier, Amsterdam.

Nemcok, M. 1995. Representation of tectonic stress. *Geol. Carpathica* **46**, 13–17.

Nemcok, M., Gayer, R. A. & Miliorizos, M. 1995. Structural analysis of the inverted Bristol Channel Basin: implications for the geometry and timing of the fracture permeability. In *Basin Inversion* (edited by Buchanan, J. G. & Buchanan, P. G.) *Spec. Publs. geol Soc.* **88**, 355–392.

Roberts, D. G. 1989. Basin inversion in and around the British Isles. In *Inversion Tectonics* (edited by Cooper, M. A. & Williams, G. D.) *Spec. Publs. geol. Soc.* **44**, 123–129.

Robertson, E. C. 1967. Laboratory consolidation of carbonate sediment. In: *Marine Geotechnique* (edited by Richards, A. F.) University of Illinois Press, Urbana.

Singh, R. N. 1976. Measurement and analysis of strata deformation around mining excavations. Unpublished Ph.D. Thesis, University of Wales, Cardiff.

Stoneley, R. & Selley, R. C. 1986. *A Field Guide to the Petroleum Geology of the Wessex Basin*. Imp. Coll. of Sci. and Tech., London, pp. 1–44.

Telford, W. M., Geldart, L. P., Sheriff, R. E. & Keys, D. A. 1976. *Applied Geophysics*. Cambridge Univ. Press.

Thomas, G. E. 1962. Grouping of carbonate rocks into textural and porosity units for mapping purposes. In *Classification of Carbonate Rocks* (edited by Ham, W. E.) AAPG Mem. No. **1**, 193–223

Van Hoorn, B. 1987. The South Celtic Sea/Bristol Channel Basin: origin, deformation and inversion history. *Tectonophysics* **137**, 309–334.

Waters, R. A., Lawrence, D. J. D., Ivimey-Cook, H. C., Mitchell, M., Warrington, G., White, D. E. & Lewis, M. A. 1987. *Geology of the South Wales Coalfield, Part II, the Country around Cardiff*. Memoir for 1:50 000 geological sheet 263 (England and Wales), Third ed., Mem. British Geol. Surv.

Weedon, G. P. & Jenkyns, H. C. 1990. Regular and irregular climatic cycles and the Belemnite Marls (Pliensbachian, Lower Jurassic Wessex Basin). *J. geol. Soc. Lond.* **147**, 915–918.

Wilcox, R. E., Harding, T. P. & Seely, D. R. 1973. Basic wrench tectonics. *Bull. Am. Ass. Petrol. Geol.* **57**, 74–96.

Wobber, F. J. 1965. Sedimentology of the Lias (Lower Jurassic) of South Wales. *J. sedim. Petrol.* **35**, 683–703.

Worden, R. H. & Smalley, P. C. 1993. Making water in deep carbonate sour gas fields. In: *Geofluids '93, Contributions to an International Conference on Fluid Evolution, Migration and Interaction in Rocks* (edited by Parnell, J., Ruffell, A. H. & Moles, N. R.) British Gas, ext. abs. 21–25.

Ziegler, P. A. 1989. Geodynamic model for Alpine intra-plate compressional deformation in Western and Central Europe. In: *Inversion Tectonics* (edited by Cooper, M. A. & Williams G. D.) Spec Publs. geol. Soc. **44**, 63–85.